ELSEVIER

Journal of Fluids and Structures 26 (2010) 74–91

JOURNAL OF FLUIDS AND STRUCTURES

www.elsevier.com/locate/jfs

Numerical analysis of active chordwise flexibility on the performance of non-symmetrical flapping airfoils

W.B. Tay*, K.B. Lim

Department of Mechanical Engineering, National University of Singapore, 21 Lower Kent Ridge Road, Singapore 119077, Singapore

Received 25 September 2008; accepted 8 October 2009
Available online 4 January 2010

Abstract

This paper investigates the effect of active chordwise flexing on the lift, thrust and propulsive efficiency of three types of airfoils. The factors studied are the flexing center location, standard two-sided flexing as well as a type of single-sided flexing. The airfoils are simulated to flap with four configurations, and the effects of flexing under these configurations are investigated. Results show that flexing is not necessarily beneficial for the performance of the airfoils. However, with the correct parameters, efficiency is as high as 0.76 by placing the flexing centre at the trailing edge. The average thrust coefficient is more than twice as high, from 1.63 to 3.57 with flapping and flexing under the right conditions. Moreover, the single-sided flexing also gives an average lift coefficient as high as 4.61 for the S1020 airfoil. The shape of the airfoil does alter the effect of flexing too. Deviating the flexing phase angle away from 90° does not give a significant improvement to the airfoil's performance. These results greatly enhance the design of a better performing ornithopter wing.

Keywords: Flapping; Non-symmetrical; Flexible; Ornithopter; Airfoil; Micro-aerial vehicle

1. Introduction

In recent years, micro-aerial vehicles (MAVs) are becoming increasingly important, especially in the area of military surveillance. MAVs can be classified into fixed wing, rotary or flapping wing MAVs. In terms of maneuverability and efficiency (η) at this low Reynolds number (Re) regime, flapping wing MAVs have a clear advantage. This phenomenon spawns an interest in research on flapping airfoils.

Initially, the research was carried out using rigid airfoils or wings. Recently, more and more studies focus on using flexible airfoils or wings. This is because in nature, the fins of fishes and wings of birds or insects are flexible. Hence, one speculates that there must be some advantages in flexible airfoils compared to their rigid counterparts. Indeed, several researches show an increase in either efficiency or thrust when the airfoils or wings exhibit active or passive flexibility. Moreover, with the advent of smart materials such as shape memory alloys (Jardine et al., 1996), one can actively control the deformation of a wing. This enables an aircraft to deform its wings according to the flight requirements to improve the aircraft's performance.

*Corresponding author. Tel.: +65 6516 6076.
E-mail addresses: Tayweebeng@nus.edu.sg, zonexo@gmail.com (W.B. Tay).

0889-9746/$ - see front matter © 2009 Elsevier Ltd. All rights reserved.
doi:10.1016/j.jfluidstructs.2009.10.005

Nomenclature

a_f	flexing displacement, nondimensionalized by airfoil chord
$\overline{a}_f$	nominal flexing displacement, nondimensionalized by airfoil chord
c	airfoil chord length
C_p	pressure coefficient
C_l	lift coefficient
$\overline{C}_l$	average lift coefficient
C_t	thrust coefficient
$\overline{C}_t$	average thrust coefficient
f	frequency, Hz
h	instantaneous heaving position, nondimensionalized by airfoil chord
h'_0	heaving amplitude
h_0	heaving amplitude, nondimensionalized by airfoil chord
h_{lf}	leading edge flexed length, perpendicular to airfoil's chord line, nondimensionalized by airfoil chord
h_{tf}	trailing edge flexed length, perpendicular to airfoil's chord line, nondimensionalized by airfoil chord
k	reduced frequency, f_c/U_∞
L	nondimensional lift force
M	nondimensional moment created by the lift and drag forces at the pitching axis
p	nondimensional pressure force
P	power input
Re	Reynolds number
St	Strouhal number, fh'_0/U_∞
t	nondimensionalized time, $t'U_\infty/c$
t'	time
t_0	time when flapping starts, nondimensionalized
T	nondimensional thrust force
u	velocity, nondimensionalized by U_∞
U_∞	freestream velocity
v_{sa}	space-averaged streamwise velocity at the exit, nondimensionalized by U_∞
x_{fc}	distance from the flex center to the leading edge, nondimensionalized by airfoil chord
x_i	Cartesian coordinates, nondimensionalized by airfoil chord
x_{lf}	distance from point of flexing to flex center, nearer the leading edge, nondimensionalized by airfoil chord
x_{tf}	distance from point of flexing to flex center, nearer the trailing edge, nondimensionalized by airfoil chord
β_{lf}	angle rotated due to leading edge flexing, in degrees
β_{lf}	angle rotated due to trailing edge flexing, in degrees
η	propulsive efficiency
θ	instantaneous pitch angle, in degrees
θ_0	pitch amplitude, in degrees
ϕ	phase difference between pitching and heaving, in degrees
ψ_f	phase angle between plunging and flexing of airfoil, in degrees

Tang et al. (2007) found from their numerical study that, as the airfoil became more flexible, a higher thrust coefficient and smaller lift coefficient were generated. The passive deformation of the airfoil due to its flexibility created a phase difference relative to its pitching motion. Another interesting result was that the detailed airfoil shape was of secondary importance compared to the equivalent angle of attack. In other words, a rigid and a flexible airfoil could give the same performance as long as both their pitching angles are equivalent throughout the flapping cycle. However, it must be emphasized that the shape of the airfoil used was a flat plate with rounded edges and the Reynolds number (Re) used was 100. It still remains to be seen what will happen if the airfoil shape is more complicated, for example, a NACA4404 airfoil.

Miao and Ho (2006) investigated the influence of flexing displacement on the aerodynamic performance of the flapping airfoil using Fluent (a commercial CFD code). They experimented with different flexing displacements, a_f ranging from 0.0 to 0.7 and found that at $\mathrm{Re} = 10^4$, $k = 2$ and $h_0 = 0.4$, a flexing displacement of 0.3 resulted in the highest propulsive efficiency. The result showed that there is a particular amount for flexing which could give optimal efficiency. Moreover, an excessive amount of flexing was actually detrimental to the efficiency. Miao and Ho's (2006) simulation also had only two parameters, namely the flexing displacement and flexing phase angle. There are still many more parameters such as the location of flexing which are not investigated. The airfoil used is a NACA0014 and other types of airfoil shape may also be used.

Zhu (2007) carried out a fully coupled fluid–structure interaction study to investigate the effect of chordwise and spanwise flexing on a flapping foil. The foil was simulated to be immersed in two different types of fluids of high and low density. It was found that in a low-density fluid, the chordwise flexibility reduced both the thrust and efficiency, while the spanwise flexibility increased the thrust without reducing efficiency within a small range of structural parameters. On the other hand, in a high-density fluid, chordwise flexibility increased the efficiency while spanwise flexibility reduced the thrust and efficiency. Hence, depending on the type of application, that is, in the air or underwater, the relevant type of flexing could be employed.

Table 1
A comparison between the two studies.

Miao and Ho's (2006) study	Current study
Only a symmetrical NACA0014 airfoil is tested	A symmetrical NACA0012 airfoil and two other non-symmetrical airfoils, NACA6302 and S1020 are tested
Airfoil undergoes a heaving flapping configuration	Airfoil undergoes a total of four flapping configurations including the heaving motion
A single flexing centre location	Three different flexing centre locations
One-directional flexing displacement	Twin directional flexing displacement
Standard flexing	Standard flexing and a special type of single-sided flexing

Pederzani and Haj-Hariri (2006) modelled an airfoil partially with membrane to allow flexing. The numerical study showed that this type of airfoil was more flexible. Moreover, another interesting result was that heavier airfoils were even more efficient than lighter ones. Unfortunately, using heavier wings would increase the overall weight of an airplane; hence it might not be as beneficial as it seemed. One had to weigh the benefit of using a heavier wing to improving efficiency.

Heathcote and Gursul (2007) used a water tunnel to investigate the effect of chordwise flexibility on a plunging airfoil at Re from 0 to 27 000. The thrust coefficient increased for airfoil of intermediate flexibility. This further confirmed the earlier simulation result by Miao and Ho (2006) that there is an optimal amount of flexing for maximum performance. Another water tunnel experiment by Heathcote et al. (2008) studied the effect of spanwise flexibility on the thrust, lift and efficiency of a heaving rectangular wing. For Strouhal number (St) >0.2, a degree of spanwise flexibility was found to increase the thrust and efficiency. However, a far greater degree of flexibility was found to be detrimental. Therefore, similar to chordwise flexing, there is also an optimal amount of flexing displacement for spanwise flexing.

The current study aims to investigate how the flexing of the airfoil affects its aerodynamic performance during flapping at a Re of 10 000, which is the flow regime for MAVs. Miao and Ho (2006) have conducted a similar study in which different flexing displacements are prescribed and tested. In their study, they simulated a flexible symmetrical NACA0014 airfoil undergoing simple heaving motion. The flexing centre location is fixed at the leading edge of the airfoil. The current study differs from Miao and Ho's (2006) in five ways. Table 1 compares the differences between the two studies.

Hence, the parameter space is now much larger, compared to that in Miao and Ho's (2006) study. It is thus more realistic because general non-symmetrical airfoils and different types of flapping motions which include pitching/heaving are considered. These additional parameters will further improve the performance of the flapping airfoil. Hence, better ornithopters which carry heavier payload and have longer endurance can be designed.

2. The incompressible flow solver

2.1. Basic algorithm

The viscous flow around the flapping airfoil is computed using the incompressible Navier–Stokes equations in the Arbitrary–Lagrangian–Eulerian (ALE) (Hirt et al., 1997) formulation,

$$\frac{\partial u_i}{\partial t}+\frac{\partial}{\partial x_j}(u_i(u-u_b)_j)=\frac{\partial p}{\partial x_i}+\frac{1}{\mathrm{Re}}\frac{\partial}{\partial x_j}\frac{\partial}{\partial x_j}u_i, \tag{1}$$

$$\frac{\partial u_i}{\partial x_i}=0, \tag{2}$$

where x_i are the Cartesian coordinates and u_i are the corresponding velocity components. u_b refers to the grid velocity.

The equations are solved using the fractional step method on structured C-grids and it is based on the method by Kim and Choi (2000). The only difference between the current solver and that of Kim is that in order to accommodate the flapping airfoil, the ALE formulation is used instead of the original formulation. No turbulence model is used due to the low Re used for the simulation.

The freestream velocity U_∞ is 1.0. The motion of the airfoil is specified by

$$h = h_0 \sin(2\pi f(t-t_0)-\phi), \tag{3}$$

$$\theta = \theta_0 \sin(2\pi f(t-t_0)). \tag{4}$$

The centre of pitch rotation is fixed at 0.25 units from the leading edge of the airfoil. The system of linear equations obtained from the momentum and Poisson equations are solved using PETSc (Balay et al., 2008), a linear equation solver and hypre (Falgout et al., 2006), a multigrid solver, respectively. The code is written entirely using Fortran90.

The boundary conditions used are (Pauley et al., 1990):

$$\textit{Inflow boundary} : u_x = u_\infty = 1, u_y = 0, dp/dx = 0; \tag{5}$$

$$\textit{Top/bottom boundary} : u_y = 0,\ du_x/dy = 0,\ dp/dy = 0; \tag{6}$$

$$\textit{Outflow boundary} : \frac{\partial u_i}{\partial t} + v_{sa}\frac{\partial u_i}{\partial x} = 0,\ p = 0. \tag{7}$$

More details about the solver can also be found in Tay (2009).

2.2. Force coefficients and efficiency computation

Since the Navier–Stokes equations have been nondimensionalized, the thrust (C_t), lift (C_l), and pressure coefficients (C_p) are

$$C_t = 2T,\ C_l = 2L,\ C_p = 2p. \tag{8, 9, 10}$$

The nondimensional thrust (T), lift force (L), and pressure (p) are the outputs from the simulation program. Due to the conformal C-grid, the thrust and lift due to the pressure and viscous forces are obtained on the surface of the airfoil and then summed up. The power input $P(t)$ can be defined as the amount of energy imparted to the airfoil to overcome the fluid forces. It is given by

$$P(t) = -L(t)\frac{dh}{dt} - M(t)\frac{d\theta}{dt}; \tag{11}$$

$M(t)$ is the moment created by the lift and drag forces at the pitching axis. Propulsive efficiency, η, which is a measure of the energy lost in the wake versus energy used in creating the necessary thrust, is given by

$$\eta = \frac{\overline{C}_t}{\overline{P}}. \tag{12}$$

2.3. Extension of flexing capability

The flexing of the airfoil is similar to the method used by Miao and Ho (2006). In their paper, they use the symmetrical NACA0014 airfoil. The airfoil is only configured to heave, but it pitches due to the flexing of the airfoil's tail. The instantaneous profile of the airfoil is described by

$$y = a_f x_{tf}^2 \cos(2\pi f(t-t_0) + \psi_f), \tag{13}$$

where a_f, x_{tf} and ψ_f denote the flexing displacement, distance from the point on the chord line to the leading edge and flexing phase angle, respectively. Eq. (13) refers to the local x–y body coordinate system. In this study, ψ_f is fixed at $\pi/2$ initially. Both a_f and x_{tf} have been nondimensionalized with the airfoil chord c.

However, as mentioned in the Section 1, the current study involves more parameters as well as the use of non-symmetrical airfoils. Hence, Eq. (13) is insufficient to represent it. The new equations are given by

$$h_{lf} = a_f (x_{lf})^2 \cos(2\pi f(t-t_0) + \psi_f), \quad h_{tf} = a_f (x_{tf})^2 \cos(2\pi f(t-t_0) + \psi_f), \tag{14, 15}$$

$$\beta_{lf} = -2\sin^{-1}(h_{lf}/2x_{lf}), \quad \beta_{tf} = 2\sin^{-1}(h_{tf}/2x_{tf}); \tag{16, 17}$$

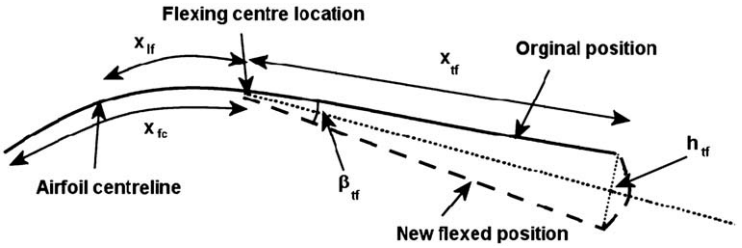

Fig. 1. Diagram of the airfoil's trailing edge flexing.

Table 2
Flexing displacement problem as flexing center moves from the leading edge to the trailing edge.

a_f	x_{fc}	a_f(old method) or a_{tf}(new method)	x_{tf}(at trailing edge)	$a_f(x_{tf})^2$
Not applicable (Old method)	0.00	0.30	1.00	0.300
	0.75	0.30	0.25	0.019
0.3 (New method)	0.75	4.80	0.25	0.300

β_{lf} and β_{tf} will be used to calculate the amount of curvature of the airfoil. Fig. 1 shows the airfoil's trailing edge flexing. Moreover, a form of "single-sided" flexing is also investigated. In this form of flexing, the airfoil only flexes in one direction, instead of two. The equations are given by

$$h_{lf} = -a_f(x_{lf})^2\left|\cos(2\pi f(t-t_0)+\psi_f)\right|, \quad h_{tf} = -a_f(x_{tf})^2\left|\cos(2\pi f(t-t_0)+\psi_f)\right| \tag{18, 19}$$

One problem which arises involves the degree of the flexing when the flexing centre changes. This is illustrated in Table 2 under the old method. From Table 2, with the same a_f, the degree of flexing at the trailing edge of the airfoil becomes much smaller (0.019) as the flexing centre point, x_{fc} moves from the leading edge to the $^3/_4$ position of the airfoil centreline. The proposed correction is to define a new nominal flexing displacement, given by $\overline{a}_f$. The relationships between the nominal and original displacements are given by

(i) for locations on the airfoil before flexing center, nearer the leading edge

$$\overline{a}_f = a_f(x_{fc})^2 \text{ for leading edge flexing;} \tag{20}$$

(ii) for locations on the airfoil after flexing center, nearer the trailing edge

$$\overline{a}_f = a_f(1.0-x_{fc})^2 \text{ for trailing edge flexing.} \tag{21}$$

This will ensure that the amount of flexing will be similar for the same $\overline{a}_f$, as shown in Table 2. The flexing displacement at the leading and trailing edge locations is exactly the same (0.3). Due to the quadratic nature of the formulas, the flexing displacement at other locations on the airfoil will be slightly different. Moreover, the a_f at the leading and trailing edge will now be different for the same $\overline{a}_f$. The new slightly modified equations are given by

$$h_{lf} = \frac{\overline{a}_f}{(x_{fc})^2}(x_{lf})^2\cos(2\pi f(t-t_0)+\psi_f), \qquad h_{tf} = \frac{\overline{a}_f}{(1.0-x_{fc})^2}(x_{tf})^2\cos(2\pi f(t-t_0)+\psi_f), \tag{22, 23}$$

$$h_{lf} = -\frac{\overline{a}_f}{(x_{fc})^2}(x_{lf})^2\left|\cos(2\pi f(t-t_0)+\psi_f)\right|, \qquad h_{tf} = -\frac{\overline{a}_f}{(1.0-x_{fc})^2}(x_{tf})^2\left|\cos(2\pi f(t-t_0)+\psi_f)\right|. \tag{24, 25}$$

The grids for the simulation are generated using the software Pointwise Gridgen. Fig. 2 shows an example of the grid. In order to simulate the flexed airfoil, the grid is deformed using arc-length-based transfinite interpolation (Jones and Samareh-Abolhassani, 1995). The space conservation law, proposed by Demirdzic and Peric (1988) has been

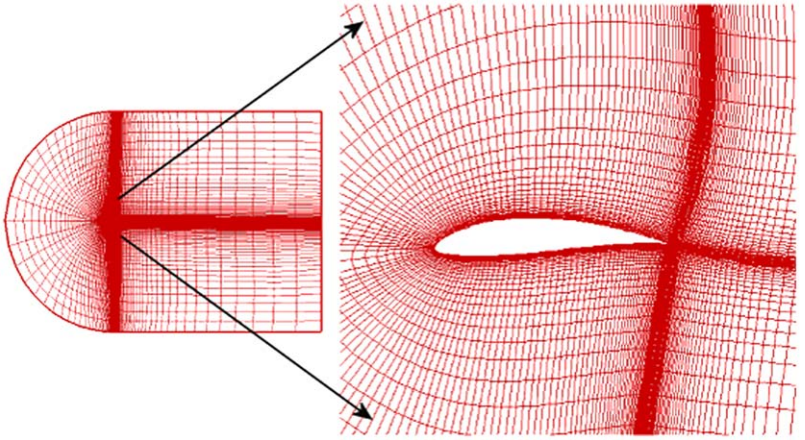

Fig. 2. An example of the 240×80 C-grid.

incorporated to consistently compute the cell area for the moving boundary. The entire new grid then rotates or translates in the x or y directions depending on the pitching and heaving requirement.

Due to the flexing of the airfoil, the angle of attack of the airfoil still changes throughout the cycle, even though the airfoil only executes heaving motion. The angle of attack is defined as angle the chord line makes with the horizontal.

2.4. Verification of solver

The solver's accuracy has been validated using four different tests in Tay and Lim (2009) and Tay (2009). These tests include efficiency (η), thrust (C_t), lift (C_l) coefficients and vorticity diagrams in comparison with simulated and experimental results. The reader can refer to the paper or thesis to obtain more details about the verifications. Grid convergence test has also been carried out. For quantitative force measurements, the 240×80 grid will be used. The first normal grid point for the grid is 3.0×10^{-4} chord lengths from the surface. Alternatively, the 1200×160 grid with the first normal grid point 6.0×10^{-4} chord lengths from the surface is used when there is a need to visualize the vorticity and pressure coefficient diagram. As explained in the paper by Tay and Lim (2009), a higher level of grid refinement is required to obtain the vorticity diagram of the simulation, compared to the aerodynamic forces. Interestingly, the grid resolution is much more important than the first normal grid point when visualizing vorticity diagrams. Therefore, all the simulations are first computed using the 240×80 grid. Whenever it is necessary to visualize the vorticity diagram for a particular configuration, the configuration will be simulated again using the 1200×160 grid.

In order to ensure that the morphing of the airfoil is done correctly, some of the tests found in the paper by Miao and Ho (2006) are repeated using the current solver. Table 3 shows a comparison of the results. Both groups of results for η and maximum C_t are very similar. However, the current solver gives a higher C_l amplitude. This seems plausible because, as given in Eqs. (11) and (12), the η is related to both the C_t and C_l. If both the η and C_t values are the same for both studies, then the C_l value should also be the same.

3. Design methodology

The airfoils tested are the NACA0012, NACA6302 and the Selig S1020 airfoils. These airfoils were used in the simulation of non-symmetrical airfoils under different flapping configurations in the paper by Tay and Lim (2009). The NACA6302 and S1020 airfoils are selected because they represent the "thin" and "thick" classes of airfoils, respectively, and they are shown in Fig. 3. The flexing will be tested based on four flapping configurations. The first configuration is the heaving motion used by Miao and Ho (2006). As a result, a direct comparison will be made between the current results and Miao and Ho's. The next three configurations are selected from the non-symmetrical airfoil simulation results by Tay and Lim (2009) which give the maximum η (ME), $\overline{C}_t$ (MT) and $\overline{C}_l$ (ML) out of the 25 flapping configurations simulated. The parameters used in these configurations are given in Table 4. The objective is to see if the flexing of the airfoils will further improve the already optimal results.

Table 3
Comparison between Miao and Ho's and current solver's results.

	Miao and Ho's solver (estimated)			Current solver		
a_f	0.00	0.10	0.30	0.00	0.10	0.30
η	0.22	0.28	0.30	0.20	0.26	0.33
Maximum C_T	0.58	0.60	0.60	0.64	0.64	0.57
Maximum C_L	3.20	2.60	1.80	4.08	3.19	1.88

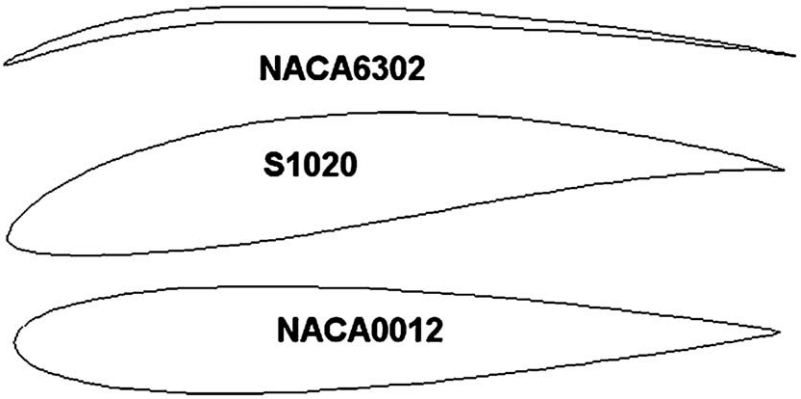

Fig. 3. Shape of the three different airfoils.

Table 4
Parameters of the different test cases.

Type	k	St	θ_0	ϕ	$h_0(=\mathrm{St}/(2k))$
Pure heaving (PH)	0.32	0.25	0.0	NA[a]	0.40
Maximum η (ME)	0.20	0.30	30.0	90	0.75
Maximum $\overline{C}_t$ (MT)	0.60	0.50	17.5	120	0.42
Maximum $\overline{C}_l$ (ML)	1.00	0.30	17.5	120	0.15

[a]NA = Not applicable.

The parameters selected are centre of flexing, leading edge flexing and trailing edge flexing. The leading edge, center of airfoil and trailing edge will be chosen as the three center of flexing locations. In order to reduce the number of simulations required, the tests are conducted based on the following procedure and criteria.

1. Begin the simulation with the smallest flexing displacement and increase the flexing in equal divisions of 0.1 each, in either direction (positive or negative).
2. When $\eta<0$, the simulation will stop immediately.
3. For $|\overline{a}_f| \leq 0.4$, the particular set of simulation will stop if the η, $\overline{C}_t$and $\overline{C}_l$ all continue to decrease consecutively after two increments.
4. For $|\overline{a}_f| > 0.4$, as long as at least one variable increases, the simulation will still continue. The simulation will stop if the η, $\overline{C}_t$and $\overline{C}_l$ all decrease after one increment.
5. The range of the parameters' degrees for a new set of simulation will change depending on the results of the previous sets of simulation.
6. If the performance of a particular flexing configuration is excellent, it will be repeated by varying itsψ_f between 60° to 120°.
7. In some cases, the grid will be distorted when the flexing displacement is too high. As a result, the solution will diverge. Due to this limitation, the range of the $\overline{a}_f$or ψ_f tested has to be decreased.

4. Results and discussion

The above-mentioned Navier-Stokes solver is used to simulate these test configurations. For each configuration, the simulation will stop once the lift and drag coefficient have reached a periodic state. This will allow the η, $\overline{C}_t$and $\overline{C}_l$ to be computed.

As mentioned in the paper by Tay and Lim (2009) for some test configurations, the lift and drag coefficients do not reach a steady periodic state. The reason is that these configurations are truly unsteady. In these cases, the η, $\overline{C}_t$ and $\overline{C}_l$ are computed over at least ten periods.

Due to the numerous cases simulated, the results are summarized in Tables 5–8. Only graphs showing the effect of $\overline{a}_f$ on η, $\overline{C}_t$and $\overline{C}_l$ for more interesting flapping configurations will be shown in this paper. They are shown from Figs. 4–7. Their results will be discussed in details in the following sections. The less important cases can be found in the thesis by Tay (2009).

4.1. Flexing – Pure heaving (h_0=0.4, k=0.32, θ_0=0°)

4.1.1. Double-sided flexing, x_{fc}=0.0, $\overline{a}_f = 0.3$

When $x_{fc} = 0.0$, maximum η is 0.33 at $\overline{a}_f = 0.3$ for the NACA0012 airfoil. This result is very similar to the results given by Miao and Ho (2006) for the NACA0014 airfoil, which is expected because the shape of the NACA0012 airfoil is very similar to that of the NACA0014 airfoil. The vorticity diagram for the original non-flexing and the pure heaving cases are shown in Fig. 8(a) and b respectively. The unflexed case generates bigger and less orderly vortices compared to the flexed case. Hence, the η of the flexed case is better.

4.1.2. Double-sided flexing, x_{fc}=1.0, 60°<ψ_f<120°

At $x_{fc} = 1.0$, maximum η of 0.66 is achieved by the NACA0012 airfoil when $x_{fc} = 1.0$ and $\overline{a}_f = -0.4$. This η of 0.66 is twice as high as the previous maximum η result (0.33). The other two airfoils also give very high η, especially the S1020 airfoil. The S1020 airfoil is able to reach an η of 0.76 at = 1.0 and $\overline{a}_f = -0.5$.

Table 5
Summarized results of the effect of flexing on the pure heaving flapping configuration.

Type of flapping configuration	Graphs shown	Summarized results
Pure heaving ($h_0 = 0.4$, $k = 0.32$, $\theta_0 = 0°$), double-sided	Fig. 4 (η)	At $x_{fc} = 0.0$ case, as the $\overline{a}_f$ increases, the $\eta$of all airfoils increase till a maximum value, after which they decrease. Similarly, at $x_{fc} = 1.0$, $\eta$of airfoils increase as $\overline{a}_f$ decreases. Hence, the airfoils in the $x_{fc} = 0.0$ case and $x_{fc} = 1.0$ case flex in opposite directions to achieve an increase in η. One can also consider that the effect of decreasing $\overline{a}_f$ with $\psi_f = 90°$ is equivalent to increasing $\overline{a}_f$ with $\psi_f = -90°$. In other words, ψ_f has shifted by 180°. At $x_{fc} = 0.0$, $\overline{C}_t$ either remains almost constant or drops as the flexing increases in either directions for the NACA0012 and the S1020 airfoils. At $x_{fc} = 0.5$ and 1.0, $\overline{C}_t$ increases as $\overline{a}_f$ decreases for all airfoils. Unlike the η and $\overline{C}_t$ plot, the graph of $\overline{C}_l$ against flexing displacement does not follow a parabolic trend. It is much more erratic. As mentioned in the paper by Tay and Lim (2009), $\overline{C}_l$ is more strongly affected by the airfoil shape, compared to $\eta$and $\overline{C}_t$. Hence, during flexing, the shape of the airfoil undergoes changes and this results in large changes in $\overline{C}_l$.
Pure heaving, single-sided	Fig. 5 ($\overline{C}_l$)	η decreases rapidly as flexing increases for all value of x_{fc}, except for the NACA6302 at $x_{fc} = 0.0$ case, whereby there is a very small η increase. The cause for the low η is two-fold. Firstly, $\overline{C}_t$ also decreases rapidly to give drag as flexing increases for all value of x_{fc} and so the power output is lower. Secondly, as mentioned in the earlier section, when C_l is increased, the power input will increase as well. A small numerator together with a large denominator thus results in the rapid decrease of the η. $\overline{C}_l$ increases rapidly as $\overline{a}_f$ increases for $x_{fc} = 0.0$ and as $\overline{a}_f$ decreases for $x_{fc} = 1.0$. The S1020 airfoil doing single-sided flexing at $x_{fc} = 0.0$, $\overline{a}_f = 0.3$ gives the highest $\overline{C}_l$ of 2.67.

Table 6
Summarized results of the effect of flexing on the ME flapping configuration.

Type of flapping configuration	Graphs shown	Summarized results
ME ($h_0 = 0.75$, $k = 0.2$, $\theta_0 = 30^\circ$, $\phi = 90^\circ$), double-sided	None[a]	This flapping configuration gives a high η of 0.54 to 0.61 for the different airfoils when the airfoils are rigid but flexing does not confer any benefit to the η for all cases. $\overline{C}_t$ also decreases as flexing increases for all cases except for the $x_{fc} = 0.0$, 0.5 cases with decreasing $\overline{a}_f$, where there is a small increase in $\overline{C}_t$. There is no noticeable trend for the change of $\overline{C}_l$ as flexing increases. For certain flexing configurations $\overline{C}_l$ increases. However, at other flexing configurations, the $\overline{C}_l$ decreases, even resulting in negative $\overline{C}_l$.
ME, single-sided	None	The trends observed with the ME single-sided airfoils are similar to that of the single-sided pure heaving case. The η and $\overline{C}_t$ decrease with increasing flexing. On the other hand, $\overline{C}_l$ increases as the flexing displacement increases for $x_{fc} = 0.0$, 0.5 and as the flexing displacement decreases for $x_{fc} = 1.0$. The NACA0012 and S1020 airfoils provide high $\overline{C}_l$ of more than 3 at $\overline{a}_f = 0.4$, giving better results compared to the heaving case.

[a]The results given by these graphs are of less importance and hence they are not shown. They can be found in Tay (2009).

Table 7
Summarized results of the effect of flexing on the MT flapping configuration.

Type of flapping configuration	Graphs shown	Summarized results
MT ($h_0 = 0.42$, $k = 0.6$, $\theta_0 = 17.5^\circ$, $\phi = 120^\circ$), double-sided	None	There is a small increase in η for some of the $x_{fc} = 0.5$, 1.0 cases as $\overline{a}_f$ decreases. This configuration is able to generate a high $\overline{C}_t$ of 2.10 to 2.50 for the unflexed airfoils. In this case, flexing still increases the $\overline{C}_t$ slightly. The variation of the $\overline{C}_l$ is very irregular as the amount of flexing increases. However, for some cases, such as at $x_{fc} = 0.0$, $\overline{a}_f = 0.4$ and $x_{fc} = 0.5$, $\overline{a}_f = 0.1$, the $\overline{C}_l$ can reach as high as 3.24 and 2.85 for the S1020 airfoil respectively.
MT, single-sided	Fig. 6 ($\overline{C}_l$)	As in the other single-sided test cases, $\overline{C}_l$ increases while η and $\overline{C}_t$ decrease as flexing increases. However, compared to the ME configuration and pure heaving case, η and $\overline{C}_t$ now decreases more slowly when the flexing increases. $\overline{C}_l$ is as high as 4.61 for the S1020 airfoil at $x_{fc} = 1.0$, $\overline{a}_f = -0.3$.

Table 8
Summarized results of the effect of flexing on the ML flapping configuration.

Type of flapping configuration	Graphs shown	Summarized results
ML ($h_0 = 0.15$, $k = 1.0$, $\theta_0 = 17.5^\circ$, $\phi = 120^\circ$), double-sided	Fig. 7 ($\overline{C}_t$)	The initial focus is on lift, so this group of simulations does not include the NACA0012 airfoil. There is a small increase in η for some of the $x_{fc} = 0.0$, 0.5 cases as $\overline{a}_f$ decreases. Moreover, the increase in $\overline{C}_t$ for the S1020 airfoil at $x_{fc} = 0.0$, $\overline{a}_f = 0.3$ shoots to more than twice the original value (3.57 vs. 1.63). Similarly, flexing at $x_{fc} = 0.0$ and 0.5 also lead to an increase in $\overline{C}_t$. $\overline{C}_l$ decreases for almost all cases except at $x_{fc} = 0.0$, $\overline{a}_f = 0.4$ for the S1020 airfoil, where the $\overline{C}_l$ increases slightly.
ML, single-sided	None	Due to the divergence of the solutions at $\overline{a}_f$ as small as ± 0.1 or ± 0.2, it is not possible to determine the trend of the effect of flexing in this group. However, in general, under small amounts of flexing, the η remains almost the same. $\overline{C}_t$ and $\overline{C}_l$ increase for some cases.

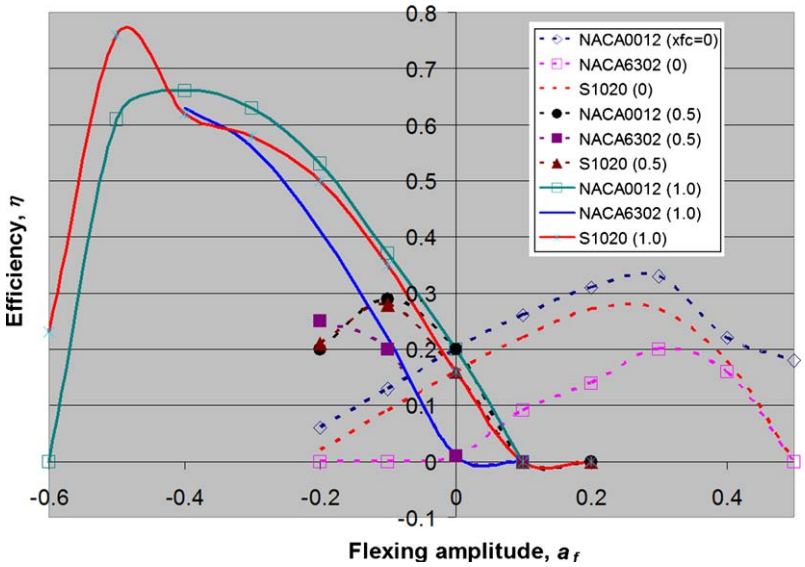

Fig. 4. Graph of η against flexing displacement for the double-sided flexing pure heaving. The thick graphs represent significant improvement due to flexing while the dotted graphs represent similar or worse performance due to flexing.

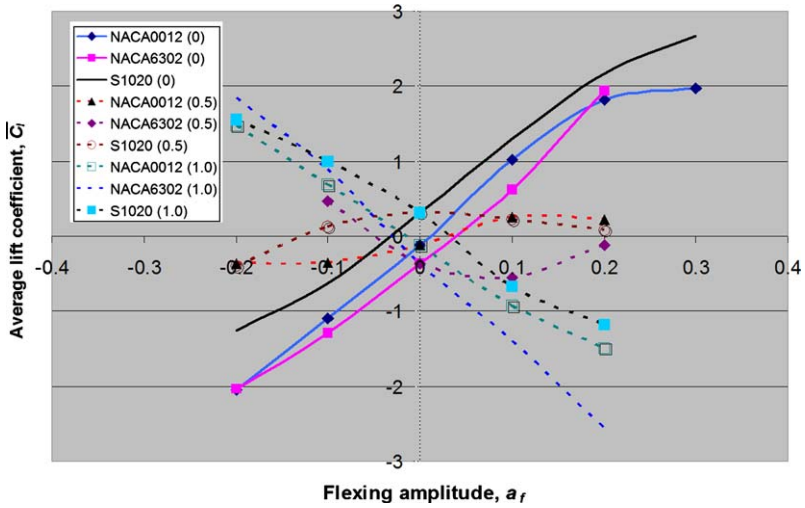

Fig. 5. Graph of $\overline{C}_l$ against flexing displacement for the single-sided flexing pure heaving.

The vorticity diagram of the NACA0012 airfoil when $x_{fc} = 1.0$ and $\bar{a}_f = -0.4$ is shown in Fig. 9(a). There is little difference in the vorticity diagram in Fig. 9(a) compared to Fig. 8(b). However, the lift amplitude of the former case (Fig. 9(a)) is approximately 1.5 compared to the latter case (Fig. 8(b)) of nearly 2.0. The definition of the power input is given in Eq. (11). The $-L(t)(\mathrm{d}h/\mathrm{d}t)$ portion of the equation usually contributes the bulk of the power input. Since the heaving amplitude is the same for both cases, the main component which determines the $P(t)$ is the C_l. Hence, when the C_l amplitude is minimized, the power input also decreases (average $P = 0.68$ at $x_{fc} = 0.0$, $\bar{a}_f = 0.3$ vs. 0.51 at $x_{fc} = 1.0$, $\bar{a}_f = -0.4$). Another factor is a higher $\overline{C}_t$ for the $x_{fc} = 1.0$ case ($\overline{C}_t = 0.34$ compared to 0.23). Higher $\overline{C}_t$ indicates higher power output (Eq. (12)). Both factors result in higher η for the $x_{fc} = 1.0$ case.

The vorticity diagram of the S1020 airfoil at $x_{fc} = 1.0$ and $\bar{a}_f = -0.5$ is shown in Fig. 9(b). It is similar to Fig. 9(a), except that the airfoil flexes even more now. The average power input/output of the S1020 and NACA0012 airfoils are 0.35/0.26 and 0.51/0.34, respectively. In other words, the unique shape of the S1020 airfoil after flexing requires much lower power input and this helps to increase the η further. At $x_{fc} = 0.5$, there is also an increase of η as $\bar{a}_f$ decreases but it is much smaller compared to the above two cases ($x_{fc} = 0.0$ and 1.0).

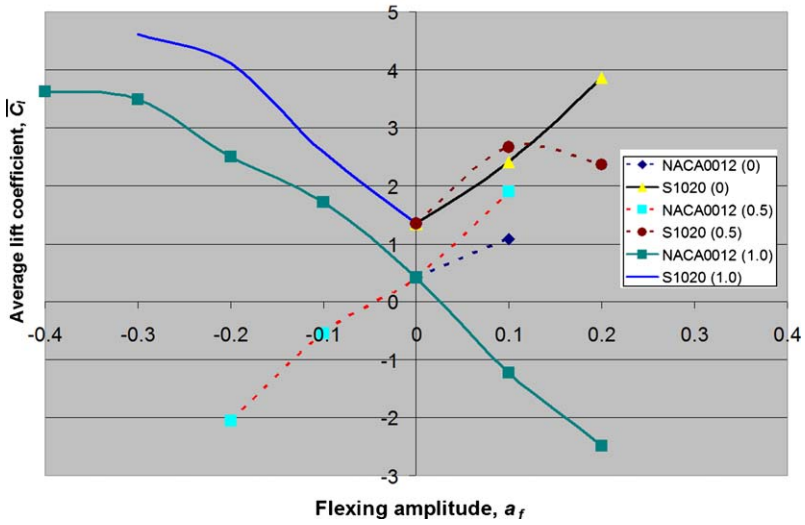

Fig. 6. Graph of $\overline{C}_l$ against flexing displacement for the single-sided flexing MT

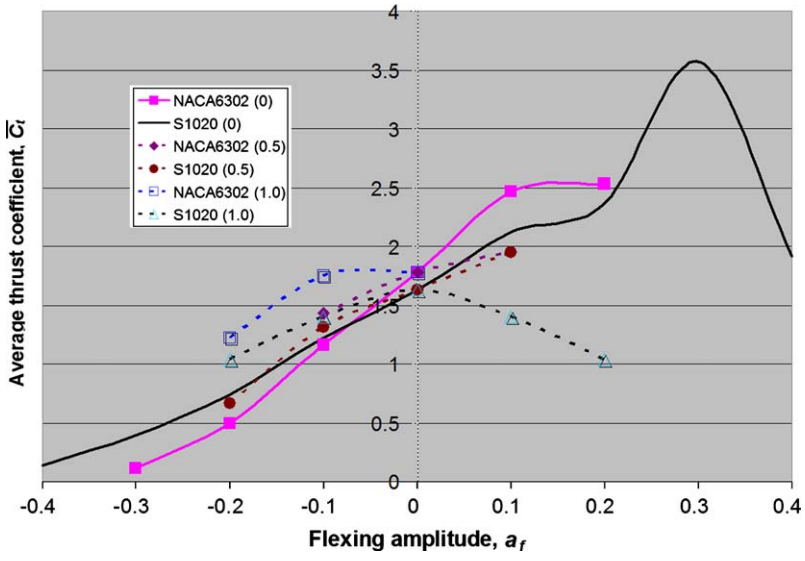

Fig. 7. Graph of $\overline{C}_t$ against flexing displacement for the double-sided flexing ML

Motivated by the high η (0.76) generated by the S1020 airfoil at $x_{fc} = 1.0$ and $\overline{a}_f = -0.5$, one wonders if changing the ψ_f can further improve the η. Hence, the simulation is repeated by varying the ψ_f from 60° to 120°. Fig. 10 shows the plot of η, $\overline{C}_t$and $\overline{C}_l$ against ψ_f. Unfortunately, there is no improvement in η and $\overline{C}_t$ as ψ_f deviates away from 90°. There is a trend of increasing $\overline{C}_l$ as ψ_f increases, albeit the increment is small.

4.1.3. Single-sided flexing, $x_{fc} = 0.0$

$\overline{C}_l$ increases rapidly as $\overline{a}_f$ increases for $x_{fc} = 0.0$ and as $\overline{a}_f$ decreases for $x_{fc} = 1.0$. However, the $x_{fc} = 0.0$ case usually gives higher η, $\overline{C}_t$ and $\overline{C}_l$ values. The S1020 airfoil doing single-sided flexing at $x_{fc} = 0.0$, $\overline{a}_f = 0.3$ gives the highest $\overline{C}_l$ of 2.67. However, the single-sided flexing S1020 airfoil is already generating a very small amount of drag ($\overline{C}_t = -0.02$) at this configuration. Similarly, the symmetrical NACA0012 airfoil also manages to give a high $\overline{C}_l$ value of 1.97 at the same flexing configuration. The pressure coefficient diagrams of the NACA0012 airfoil for the $x_{fc} = 0.0$, $\overline{a}_f = 0.2$ (with

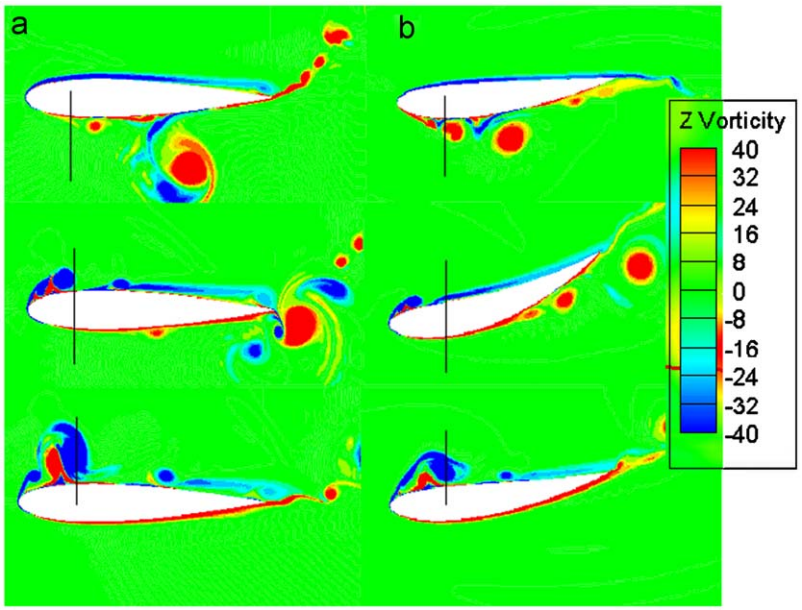

Fig. 8. Vorticity diagram of NACA0012 airfoil undergoing pure heaving (a) without flexing, and (b) with flexing at $x_{fc} = 0.0$ and $\overline{a}_f = 0.3$ during the heaving down cycle. The black vertical line in the vorticity diagram indicates the approximate peak to peak heaving amplitude. The rest of the vorticity diagrams will have the same legend as that of Fig. 8.

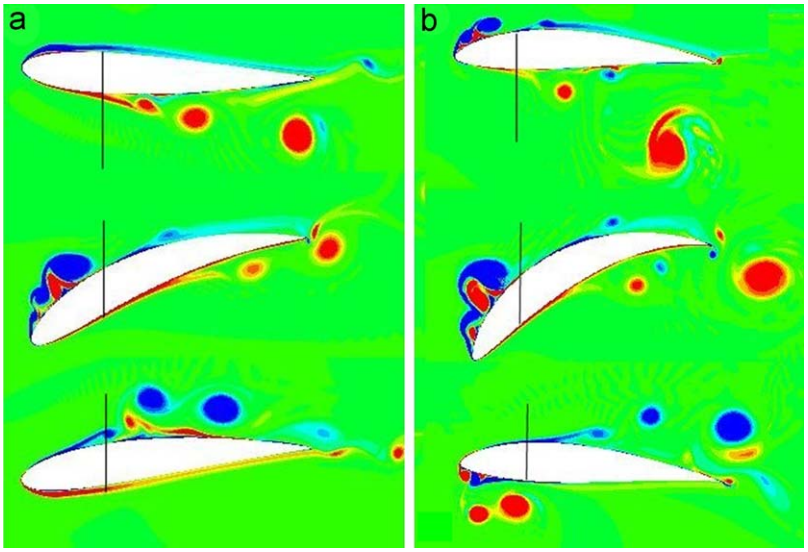

Fig. 9. Vorticity diagram of the NACA0012 airfoil (a) undergoing pure heaving with flexing at $x_{fc} = 1.0$, $\overline{a}_f = -0.4$ and the S1020 airfoil, and (b) undergoing pure heaving with flexing at $x_{fc} = 1.0$, $\overline{a}_f = -0.5$ during the heaving down cycle

$\overline{C}_t = 0.10$, $\overline{C}_l = 1.81$) are shown in Fig. 11 while the unflexed version is shown in Fig. 12. The pressure diagram in Fig. 11 shows that as the airfoil plunges down, there is a growing leading edge vortex on top of the airfoil. This creates a low pressure suction region which improves the lift coefficient generated by the airfoil greatly. This is also the time when the C_l is at its maximum ($C_l = 7.0$). Although both figures have the leading edge vortex, the magnitude of the vorticity on Fig. 11 is much larger. Moreover, the leading edge vortex stays attached to the airfoil for a longer period of time before shedding away. On heaving up, a leading edge vortex is also formed at the bottom of the airfoil for both figures. However, the vortex on Fig. 11 is much smaller and detaches after a very short while. Hence, this imbalance results in

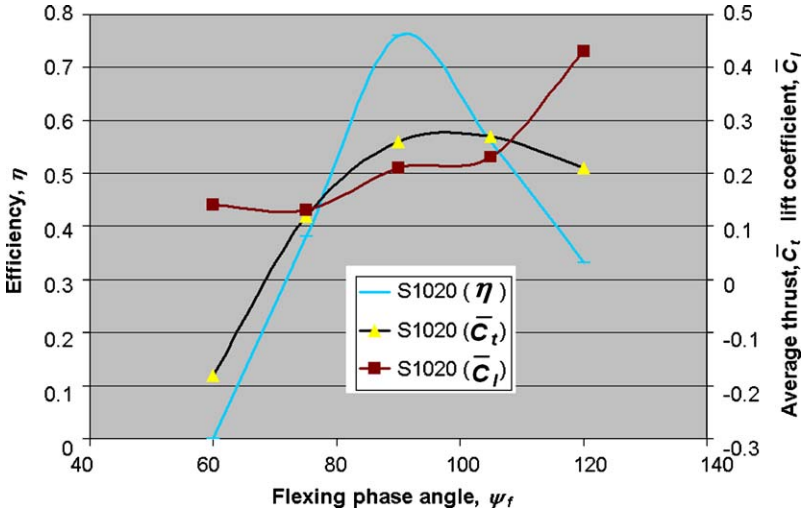

Fig. 10. Graph of η, $\overline{C}_t$ and $\overline{C}_l$ against ψ_f for the double-sided flexing pure heaving.

very high $\overline{C}_l$. On the other hand, the unflexed airfoil has similar leading edge vortices on the top and bottom of the airfoil, resulting in a very small $\overline{C}_l$.

4.2. Flexing – MT configuration (h_0=0.42, k=0.6, θ_0=17.5°, ϕ=120°)

4.2.1. Single-sided flexing, x_{fc}=1.0, $\overline{a}_f = -0.3$, 60° < ψ_f < 120°

$\overline{C}_l$ is as high as 4.61 for the S1020 airfoil at $x_{fc} = 1.0$, $\overline{a}_f = -0.3$. This is the highest $\overline{C}_l$ obtained out of all the flapping configurations simulated in this study. The simulations for the S1020 airfoil at $x_{fc} = 1.0$, $\overline{a}_f = -0.3$ is repeated by varying its ψ_f. from 60° to 120°. Fig. 13 shows the plot of η, $\overline{C}_t$and $\overline{C}_l$ against ψ_f. Varying the ψ_f does not improve the lift performance of the airfoil but there is a small increase in the η and $\overline{C}_t$ as ψ_f increases from 90° to 120°.

4.3. Flexing – ML configuration (h_0=0.15, k=1.0, θ_0=17.5°, ϕ=120°)

4.3.1. Double-sided flexing, x_{fc}=0.0, $\overline{a}_f = 0.3$, 60° < ψ_f < 120°

The increase in $\overline{C}_t$ for the S1020 airfoil at $x_{fc} = 0.0$, $\overline{a}_f = 0.3$ shoots to more than twice the original value (3.57 versus 1.63), although the η also drops to about half the original value. The graphs on Fig. 14 show the plot of η, $\overline{C}_t$and $\overline{C}_l$ against ψ_f. Similarly, there is no improvement of $\overline{C}_t$ when ψ_f diverges from 90° to 60° or 120°. However $\overline{C}_l$ increases to from 1.65 to 3.34 at $\psi_f = 75°$, but this is also accompanied by a decrease in η and $\overline{C}_t$ from 0.11 and 3.57 to 0.06 and 1.58 respectively.

4.3.2. Single-sided flexing, x_{fc}=1.0, $\overline{a}_f = -0.2$

In this case, the η and $\overline{C}_t$ are very similar to the unflexed case. Both variables do not drop as rapidly, compared to the earlier pure heaving, ME and MT configurations. η and $\overline{C}_t$ hover around 0.2 and 1.6 respectively. $\overline{C}_l$ is 4.38, compared to that of the unflexed airfoil of 1.93. The pressure coefficient diagrams of the unflexed and flexed S1020 airfoil at $x_{fc} = 1.0$, $\overline{a}_f = -0.2$ are shown in Fig. 15(a) and (b) respectively. The pressure coefficient diagrams show that the only difference lies in the presence of a leading edge vortex near the front top end of the flexed airfoil. The vortex creates a low pressure region and aids to increase the $\overline{C}_l$.

4.4. Comparison of effect of flexing between different flapping configurations

The effect of flexing is simulated on the airfoils under different flapping parameters. These include the pure heaving, ME, MT and ML configurations. Under the same flexing condition, the effect of flexing on η, $\overline{C}_t$and $\overline{C}_l$ can be very different when different flapping parameters are used. For example at $x_{fc} = 0.0$, η increases to a maximum of 0.33 as $\overline{a}_f$

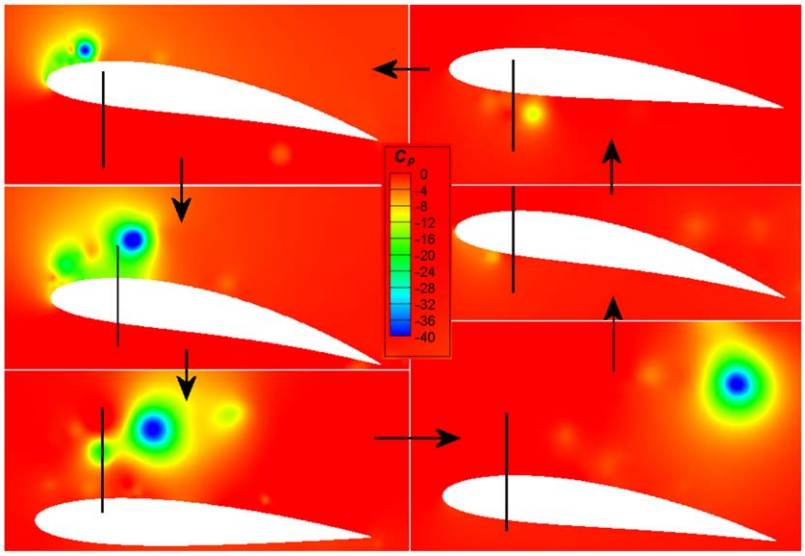

Fig. 11. Pressure coefficient diagram of the NACA0012 airfoil undergoing pure heaving with singled sided flexing at $x_{fc} = 0.0$ and $\overline{a}_f = 0.2$.

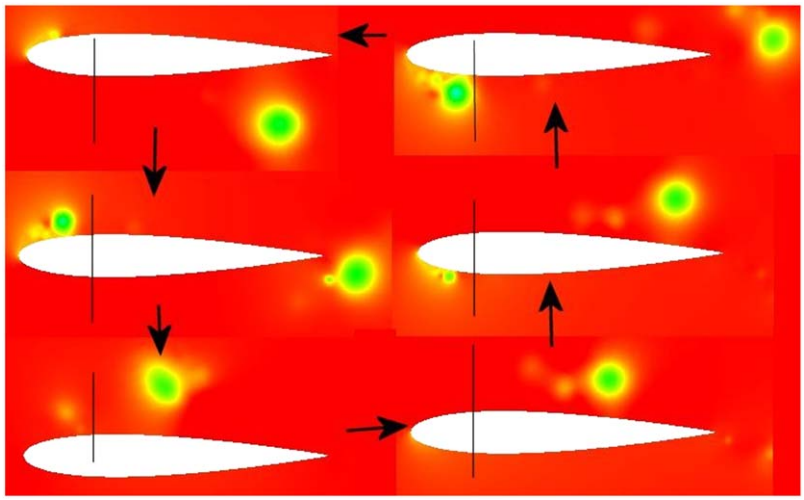

Fig. 12. Pressure coefficient diagram of the NACA0012 airfoil undergoing pure heaving without flexing (same legend as Fig. 11).

increases for the NACA0012 airfoil heaving case (Fig. 4(a)). However, for the ME configuration, η drops rapidly and produces drag at $\overline{a}_f = 0.2$

Similarly for thrust, the effect of flexing can be beneficial or detrimental. For the NACA0012 airfoil, when flapping with the ME configuration's parameters, $x_{fc} = 0.0$, $\overline{a}_f = -0.2$ produces 60% more thrust compared to the unflexed case (0.50–0.81). The flexing causes more vortices to be shed into the wake and increase the thrust. On the other hand, with the MT configuration, the same flexing parameters cause $\overline{C}_t$ to drop by 27% (2.50–1.83). The same observation is also true for the $\overline{C}_l$.

However, for the single-sided simulations, the trend is the same for all the flapping configurations except the ML configuration. The η and $\overline{C}_t$ decrease as the flexing increases. Depending on the direction of flexing, the $\overline{C}_l$ will increase or decrease. In the ML configuration, η and $\overline{C}_t$ do increase for some airfoils as the flexing increases. Of all the flapping configurations, the effect of flexing seems to benefit the MT configuration much better.

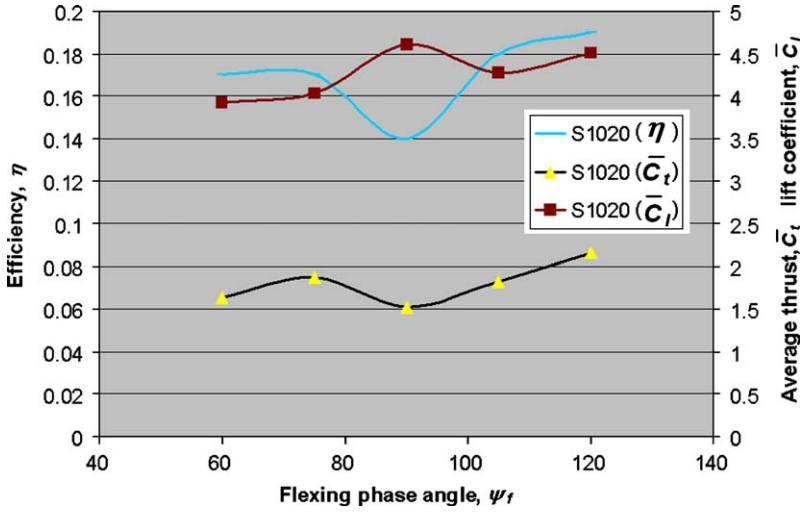

Fig. 13. Graph of η, $\overline{C}_t$ and $\overline{C}_l$ against ψ_f for the single-sided flexing MT.

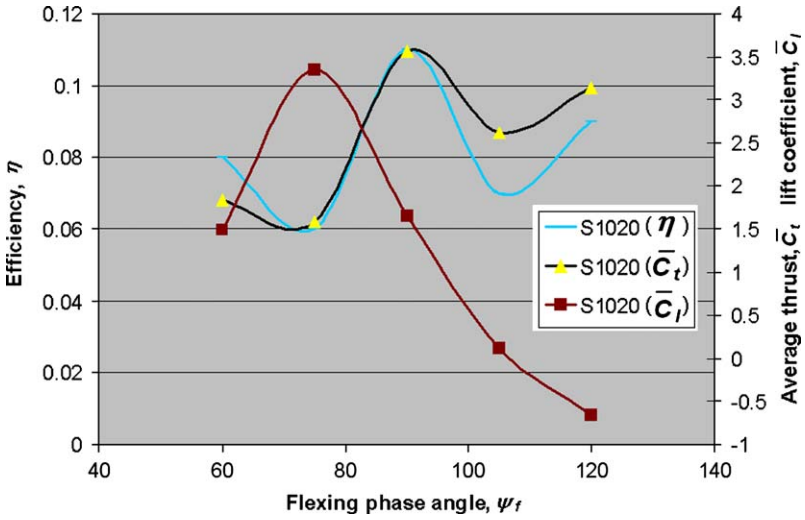

Fig. 14. Graph of η, $\overline{C}_t$ and $\overline{C}_l$ against ψ_f for the double-sided flexing ML.

4.5. Comparison of effect of flexing between different airfoils under similar flapping configurations

In the paper by Tay and Lim (2009), it was found that different airfoils produced similar $\overline{C}_t$ under the same flapping configurations. On the other hand, the $\overline{C}_l$ produced relied more on the shape of the airfoil. η is influenced both by the flapping configuration and the shape of the airfoil equally. As the flexing displacement increases, certain flapping configurations show a marked difference in $\overline{C}_t$ and η while some others do not. For example, the $\overline{C}_t$ produced by the unflexed ME configuration is very similar for the different airfoils. However, at $x_{fc} = 0.0$, $\overline{a}_f = -0.5$, the $\overline{C}_t$ produced by the NACA0012 and S1020 airfoils are 0.89 and 0.58 respectively. The difference in η between the airfoils is also larger now.

On the other hand, under the ML configuration, the η and $\overline{C}_t$ are similar for the unflexed NACA6302 and S1020 airfoils. At $x_{fc} = 0.0$, $\overline{a}_f = 0.2$, both the η of the NACA6302 and S1020 airfoils have dropped to half their original values (0.11 and 0.10) and $\overline{C}_t$ has increased to similar values (2.53 and 2.36) (Fig. 7).

For lift, different airfoils give different results. The NACA0012 airfoil generates the least $\overline{C}_l$ due to its symmetrical nature. On comparison, the S1020 airfoil performs better than the NACA6302 airfoil, especially with regards to the single-sided simulations.

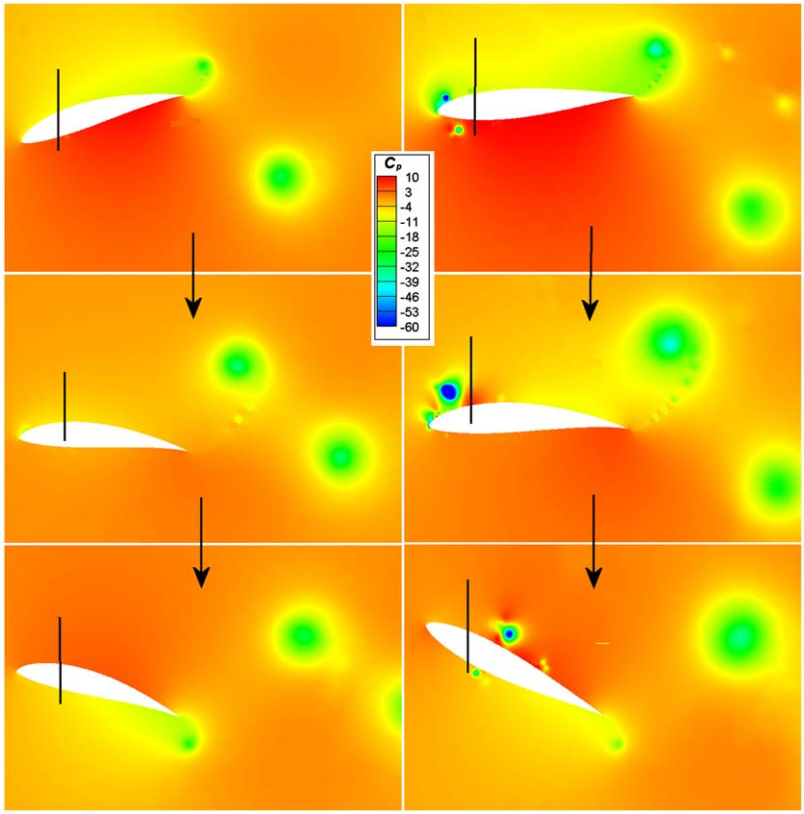

Fig. 15. Pressure coefficient diagrams of the (a) unflexed and (b) flexed S1020 airfoil at $x_{fc} = 1.0$, $\overline{a}_f = -0.2$ for the ML single-sided case.

Table 9
Simulation of NACA0012 with ME configuration at different θ_0.

θ_0(deg.)	η	$\overline{C}_t$	$\overline{C}_l$
20.0	0.50	0.61	−0.08
25.0	0.57	0.58	−0.09
30.0	0.61	0.50	0.00
35.0	0.44	0.21	−0.02
40.0	0.26	0.09	0.00

4.6. Comparison of effect of flexing and pitching

This section discusses in more details the effects of flexing compared to pitching. Results show that flexing results in a decrease in η for the ME configuration for all values of x_{fc}. As mentioned earlier in the introduction by Tang et al. (2007), the effect of flexing is similar to that of pitching. Therefore, a pitching amplitude $\theta_0 = 30^\circ$ plus a small of amount of flexing will mean a $\theta_0 > 30^\circ$. This configuration may have passed the optimum point and therefore the η is lower.

In order to test the hypothesis, the simulation is repeated using NACA0012 with ME flapping configuration at different θ_0 ranging from 20° to 40°. No flexing is involved. Table 9 shows that η is indeed optimum at $\theta_0 = 30^\circ$. Beyond that, η decreases. Hence, the effect of flexing is similar to increasing the θ_0 since both result in a decrease in η. On the

other hand, $\overline{C}_t$ decreases as θ_0 increases until almost zero at $\theta_0 = 40^\circ$ but at $x_{fc} = 0.0$, as $\overline{a}_f$ changes from 0.0 to -0.4, $\overline{C}_t$ increases up to 0.91. This shows that effect of flexing is not always equivalent to that of increasing θ_0. Pitching causes the whole airfoil to rotate as a rigid body while flexing causes different parts of the airfoil to move or rotate in different amounts. For example, if $x_{fc} = 0.0$, the leading edge of the airfoil does not move at all while the trailing edge moves by the largest amount. The resulting shape of the airfoil after flexing is different from its original unflexed shape. The resulting η, $\overline{C}_t$and $\overline{C}_l$ of the flexing of the airfoil can therefore be better (as in the above-mentioned case, higher $\overline{C}_t$) or worse than the airfoil flapping with a higher θ_0.

5. Conclusion

The simulation results show that flexing is not necessarily beneficial for the airfoils. The performance of the airfoil depends on the type of flapping configurations. For η and $\overline{C}_t$, as the flexing increases ($\overline{a}_f$ increases or decreases), these two factors either follow a parabolic or strictly decreasing trend (if flexing is detrimental to $\eta/\overline{C}_t$). Only two cases (S1020 airfoil, ME($x_{fc} = 0.0$) and NACA0012 airfoil, pure heaving($x_{fc} = 0.0$)) are exceptions. On the other hand, $\overline{C}_l$ does not follow similar trend among the different flapping configurations since it is very sensitive to the shape of the airfoil.

In certain cases, such as the pure heaving case, η is as high as 0.66 and 0.76 for the NACA0012 and S1020 airfoils, respectively. These improvements are much higher than Miao and Ho's (2006) flexible NACA0014 airfoil which is also undergoing pure heaving motion. The main differences lie in the choice of the flexing centre location and the flexing direction. The high η produced by the pure heaving case is very attractive because it is much easier to design an ornithopter which flaps in one dimension (pure heaving), compared to one which heaves, pitches and rows (movement of airfoil in forward/backward direction). In the past, it is not possible to obtain high η in a pure heaving case when the airfoil is rigid. Moreover, the simplification in the flapping mechanism design will also produce a much lighter ornithopter.

$\overline{C}_t$ increases for some of the flapping configurations when flexing occurs. The most significant increase occurs at $x_{fc} = 0.0$, $\overline{a}_f = 0.3$ for the ML (maximum lift) configuration of the S1020 airfoil where the $\overline{C}_t$ increases from 1.63 to 3.57 (Fig. 7).

The performance of lift generation is discussed only briefly in Miao and Ho's paper because a symmetrical NACA0014 airfoil undergoing pure heaving motion is simulated. This resulted in a $\overline{C}_l$ of zero. The performance of lift generation differs for different flapping configurations under standard flexing in the current study. It can be either beneficial or detrimental. However, under single-sided flexing, $\overline{C}_l$ generally increases as the amplitude increases for $x_{fc} = 0.0$, 0.5 and decreases for $x_{fc} = 1.0$. $\overline{C}_l$ is as high as 4.61 for the S1020 airfoil ($x_{fc} = 1.0$, $\overline{a}_f = -0.3$).

Flexing does not guarantee improved η, $\overline{C}_t$ or $\overline{C}_l$, such as in the ME (maximum η) case. Results show that when the airfoil is already performing at the maximum η, $\overline{C}_t$ or $\overline{C}_l$ (as in the ME, MT and ML cases), flexing will at most introduce a small amount of benefit to the respective variable. For example, for the MT case, $\overline{C}_t$ only improves by a very small amount after flexing. For some flapping configurations which give very high η, $\overline{C}_t$ or $\overline{C}_l$, the simulations are repeating by varying the flexing phase angle ψ_f from 60° to 120°. However, there is no significant improvement to give higher η, $\overline{C}_t$ or $\overline{C}_l$ in most cases.

In some cases, the shape of the airfoil also influences the effect of flexing, resulting in a difference in the results between two different airfoils flexing with the same amplitude under the same flapping configuration. In general, the S1020 airfoil gives better $\overline{C}_t$ than the NACA6302 airfoil.

By carefully controlling the flexing displacement and selecting a suitable type of flexing (single or double sided) for an airfoil, the η, $\overline{C}_t$ or $\overline{C}_l$ can be improved compared to their rigid counterparts. For example, if η is the most important criteria, the S1020 airfoil flapping at pure heaving motion with $x_{fc} = 1.0$ and $\overline{a}_f = -0.5$ is selected. This information can aid in the design of a better ornithopter's wing and hence improve the endurance and payload capability of an ornithopter.

More complexities can be added to the simulation to further improve the performance of the airfoils. In the current simulation, only three x_{fc} values are selected (0.0, 0.5 and 1.0). Other values such as $x_{fc} = 0.25$ can also be tested. The flexing displacement a_f is the same for the leading and trailing edge. However, it will be interesting to see what happen if the leading and trailing edge flexing displacement are different. Lastly, it is also possible to allow the x_{fc} to move along the chord as the airfoil is flapping. For example, when airfoil is at its highest heaving position, $x_{fc} = 0.0$. As the airfoil moves down to the lowest heaving position, x_{fc} moves from 0.0 to 1.0.

The current study simulates the airfoil in 2-D and hence studies have to be done in 3-D to give further validations. Complexities will increase because besides chordwise flexing, one also has to consider the effect of spanwise flexing. Other 3-D effects such as tip vortices may also influence the performance of the wing under flexing. Experimental studies must also be conducted. However, it must be noted that designing an actual wing which mimics the flexing is not trivial.

References

Balay, S., Buschelman, K., Eijkhout, V., Kaushik, D., Knepley, M.G., Mcinnes, L.C., Smith, B.F., Zhang, H., 2008. Petsc users manual. Technical report ANL-95/11 - Revision 3.0.0, Argonne National Laboratory.

Demirdzic, I., Peric, M., 1988. Space conservation law in finite volume calculations of fluid-flow. International Journal for Numerical Methods in Fluids 8, 1037–1050.

Falgout, R.D., Jones, J.E., Yang, U.M., 2006. The Design and Implementation of Hypre, a Library of Parallel High Performance Preconditioners. Numerical Solution of Partial Differential Equations on Parallel Computers. Springer-Verlag, pp. 267–294.

Heathcote, S., Gursul, I., 2007. Flexible flapping airfoil propulsion at low reynolds numbers. AIAA Journal 45, 1066–1079.

Heathcote, S., Wang, Z., Gursul, I., 2008. Effect of spanwise flexibility on flapping wing propulsion. Journal of Fluids and Structures 24, 183–199.

Hirt, C.W., Amsden, A.A., Cook, J.L., 1997. An arbitrary Lagrangian-Eulerian computing method for all flow speeds. Journal of Computational Physics 135, 203–216.

Jardine, A.P., Kudva, J.N., Martin, C.A., Appa, K., 1996. Shape memory alloy TiNi actuators for twist control of smart wing designs. In: Proceedings of the SPIE - The International Society for Optical Engineering, San Diego, CA, United States, pp. 160–165.

Jones, W.T., Samareh-Abolhassani, J., 1995. Grid generation system for multi-disciplinary design optimization. NASA Langley Technical Report Server United States.

Kim, D., Choi, H., 2000. A second-order time-accurate finite volume method for unsteady incompressible flow on hybrid unstructured grids. Journal of Computational Physics 162, 411–428.

Miao, J.M., Ho, M.H., 2006. Effect of flexure on aerodynamic propulsive efficiency of flapping flexible airfoil. Journal of Fluids and Structures 22, 401–419.

Pauley, L.L., Moin, P., Reynolds, W.C., 1990. The structure of 2-dimensional separation. Journal of Fluid Mechanics 220, 397–411.

Pederzani, J., Haj-Hariri, H., 2006. Numerical analysis of heaving flexible airfoils in a viscous flow. AIAA Journal 44, 2773–2779.

Tang, J., Viieru, D., Shyy, W., 2007. A study of aerodynamics of low reynolds number flexible airfoils. In: Proceedings of the Collection of Technical Papers - 37th AIAA Fluid Dynamics Conference, Miami, FL, USA, pp. 1465–1481.

Tay, W.B., 2009. Analysis of non-symmetrical flapping airfoils and their configurations. Ph.D. National University of Singapore.

Tay, W.B., Lim, K.B., 2009. Analysis of non-symmetrical flapping airfoils. Acta Mechanica Sinica 25, 433–450.

Zhu, Q., 2007. Numerical simulation of a flapping foil with chordwise or spanwise flexibility. AIAA Journal 45, 2448–2457.